# Properties of Co–Fe Films: Dependence of Cathode Potentials

Mursel Alper[1], Hakan Kockar[2], Turgut Sahin[2], and Oznur Karaagac[2]

[1]Physics Department, Science and Literature Faculty, Uludag University, Gorukle, Bursa 16059, Turkey
[2]Physics Department, Science and Literature Faculty, Balikesir University, Balikesir 10145, Turkey

**Co–Fe films were electrodeposited on Titanium substrates at the cathode potentials changing from −1.8 to −2.7 V with respect to saturated calomel electrode (SCE). The structural analysis by X-ray diffraction revealed that all films have a mixed phase of face centered cubic and body centered cubic structure, but the phase ratios change depending on the cathode potentials. The compositional analysis, which was made using an energy dispersive X-ray spectrometry, demonstrated that the Co content of the films slightly increases as the deposition potential increases. The morphological analysis of the films grown at high deposition potential (−2.7 V versus SCE), studied by scanning electron microscopy, indicate that they have larger grains. All Co–Fe films showed anisotropic magnetic resistance up to 4% and its magnitude was affected by the cathode potentials. Magnetic measurements carried out by the vibrating sample magnetometer indicated that the saturation magnetization varied and the coercivity decreased from 46.98 to 31.74 Oe as the cathode potential increased. The easy axis of magnetization was found to be in the film plane for all films. The variation in magnetoresistance and magnetic properties may be related to the structural changes in the films.**

*Index Terms*—**Electrochemical process, magnetic analysis, magnetic films, magnetoresistance (MR).**

## I. INTRODUCTION

ELECTRODEPOSITION offers a simple and low-cost way of fabricating thin film recording heads. The deposition only takes place on a conducting plate connected to the external circuit. Electrodeposited films with ferromagnetic components such as Fe, Ni, and Co have attracted much interest for a long time due to their potential applications such as magnetoresistive sensors and data storage devices [1], [2]. Magnetic recording technology requires soft magnetic materials with larger saturation magnetization, $M_s$ and lower coercivity, $H_c$ to increase storage density in magnetic recording [3]. Therefore, soft magnetic materials with higher saturation magnetizations such as Co–Fe and Co–Fe–Ni have been developed [4].

The properties of electrodeposited films show dependence on the deposition conditions. For example, the deposition potential is one of the most effective parameters. In this study, a series of Co–Fe films were produced at different cathode potentials. The structural, magnetic, and magnetotransport properties of the films were investigated as a function of the cathode potential. It was found that the different deposition potentials lead to different structural, magnetic, and magnetotransport properties.

## II. EXPERIMENT

Co–Fe alloy films were electrodeposited on Titanium (Ti) substrate from electrolyte consist of 0.5M $CoSO_4 7H_2O$, 0.1M $FeSO_4 5H_2O$, and 0.3M $H_3BO_3$ using a potentiostat (EGG model 362) with three electrodes. During the film deposition electrolyte pH was stable at $3.00\pm0.05$ and the nominal film thickness was fixed at 3 $\mu$m. The films were deposited at the cathode potentials of −1.8, −2.0, −2.3, −2.5, and −2.7 V versus saturated calomel electrode (SCE). After the deposition, the films were easily peeled off their Ti substrates mechanically. All measurements were made after removing the substrates of the films. The electrolyte was characterized by cyclic voltammetry (CV) with a scan rate of 20 mV/s. The scan
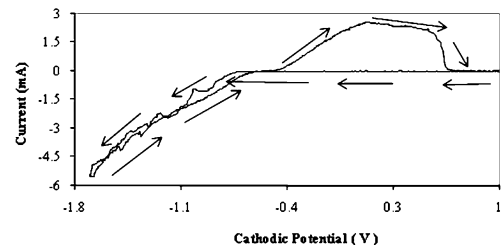
Fig. 1. CV curve of the electrolyte used for the deposition of Co–Fe films.

was performed on a Ti electrode with an area of ∼0.01 cm² in the cathodic direction from +1.0 to −1.7 V versus SCE. The deposition potential was estimated from the CV curves.

The crystal structure of the films was studied using the X-ray diffraction [(XRD) Rigaku-rint 2200] technique. The film morphology and composition was determined by scanning electron microscope (SEM) and energy dispersive X-ray (EDX) spectrometry, respectively. Magnetoresistance (MR) measurements were made at room temperature in magnetic fields range of ±10 kOe using the Van der Pauw (VDP) method with four point probes arranged in a square. Magnetic characteristics of the films were investigated with a vibrating sample magnetometer [(VSM) ADE EV9 model]. A magnetic field up to ±20 kOe was applied both parallel and perpendicular to the plane of the films.

## III. RESULTS AND DISCUSSION

In order to obtain preliminary information about the deposition processes and to start with the appropriate cathode potential, the electrolyte was first characterized by CV. Fig. 1 indicates the CV curve of the electrolyte used to deposit Co–Fe films. In the cathodic direction, in the region between +1.0 and −0.6 V, the current is almost zero. After −0.6 V, a large cathodic current starts flowing with the increase of the potential, due to the deposition of both Co and Fe ions in the electrolyte. In the anodic direction, there is a broad peak from −0.4 to 0.6 V. This peak probably indicates the dissolution of cobalt and iron. It was reported that the potential for the deposition of Co and Fe should be higher than −0.6 V [5], [6]. Based on the results obtained from the CV curve and the values in other studies [5], [6], the appropriate potential ranges to deposit Co–Fe alloys were estimated. The actual deposition potentials within these

TABLE I
STRUCTURAL, COMPOSITIONAL AND MAGNETIC ANALYSIS

| Cathode potential (V vs. SCE) | Crystal structure (XRD) | Composition (EDX) | | Magnetoresistance (MR) | | Magnetic properties (VSM) | |
|---|---|---|---|---|---|---|---|
| | Phase ratio fcc/bcc | Co (wt.%) | Fe (wt. %) | LMR (%) | TMR (%) | $H_c$ (Oe) | $M_s$ (emu/cm$^3$) |
| -1.8 | 0.68 | 78 | 22 | 1.6 | 1.3 | 46.98 | 1341 |
| -2.0 | 1.21 | - | - | 2.5 | 2.1 | 45.41 | 1254 |
| -2.3 | 1.11 | 80 | 20 | 2.9 | 2.1 | 40.35 | 1319 |
| -2.5 | 1.75 | - | - | 3.1 | 2.4 | 38.79 | 1540 |
| -2.7 | 5.04 | 83 | 17 | 4.1 | 2.4 | 31.74 | 1633 |
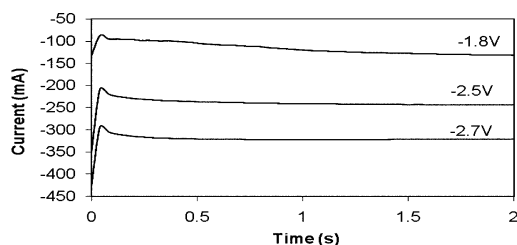


Fig. 2. Current–time transients for the films deposited at different cathode potentials.



Fig. 3. XRD patterns of the films deposited at different cathode potentials [F1: fcc (111), F2: fcc (200), F3: fcc (220), F4: fcc (311), B1: bcc (110), B2: bcc (200), B3: bcc (211)].

intervals were chosen to yield a deposit with a metallic appearance (mirror-like). Therefore, the potentials between $-1.8$ and $-2.7$ V should be selected.

The current was recorded as a function of the time to investigate the growth mechanisms of the Co–Fe films during deposition. The current-time transients of the films produced at three different cathode potential of $-1.8$, $-2.5$, and $-2.7$ V are shown in Fig. 2 for the first two seconds of deposition period. In the figure, at the beginning of the applied potentials a high cathodic current is seen for a short time and then the current steeply drops because of the depletion of the metal ion concentrations close to the electrode surface and consequently reaches a stable value [7]. The current occurred during the deposition of the film at low cathode potential is lower with respect to that of the film produced at high cathode potential. The proper films were deposited as the current values are stable for each deposition potential.

Compositional analysis of the Co–Fe films obtained from EDX spectrometers are listed in Table I. The results indicate that Co content of the films slightly and orderly increases as the cathode potential increases. As we shall see later, the film composition also plays an important role on the phase of the crystal structure. The crystal structure of the films was analyzed and their XRD patterns were given in Fig. 3. The patterns indicate that all films have a mixed phase of face-centered cubic (fcc) and body-centered cubic (bcc). As seen from the figure, the reflections from the characteristic (111), (200), (220), (311) crystal planes of fcc structure were observed at approximately $2\theta = 44°, 52°, 76°, 93°$, respectively. In addition, the (110), (200), (211) peaks of bcc phase were observed at $45°, 65°, 84°$, respectively. The fcc/bcc phase ratio was calculated using the ratio of the integral intensities of fcc peaks to those of bcc ones and is shown in Table I.

In all patterns, the integral peak intensities of fcc increases with the decrease of the bcc ones caused by the increase of the
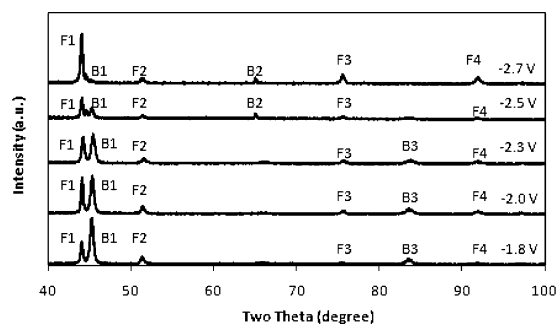
cathode potentials. At $-2.5$ V, the peak of the bcc (211) disappears whereas the bcc (200) starts to appear, as seen from Fig. 3. The bcc phase is predominant at $-1.8$ V since the fcc/bcc phase ratio is lower than 1, and the ratio increases to 5.042 as the fcc phase become increasingly dominant for the films grown at the potentials of $-2.3$ to $-2.7$ V and approximately stable at $-2.0$ and $-2.3$ V. The increase in the ratio of the fcc to the bcc phase is probably related to the increase in the Co content of the film, caused by the high deposition potential. The increase in the fcc/bcc phase ratio can be explained as the electrodeposited Co films crystallize in fcc structure.

The lattice parameters of films were calculated using the least squares technique to fit experimental data a straight line [8]. The average lattice parameter for the films was found to be $(0.2861 \pm 0.0006)$ nm for bcc phase and $(0.3556 \pm 0.0006)$ nm for fcc phase. These values are compatible with lattice parameters of Co (0.3523 nm) and Fe (0.2860 nm) [8].

Fig. 4(a) and (b) shows the SEM micrographs of the films deposited at $-1.8$ and $-2.7$ V, respectively. Morphological investigation indicated that all films have grainy structure, however, when the films are prepared at low cathode potential ($-1.8$ V), they have larger grains than those prepared at high cathode potential ($-2.7$ V). The average grain sizes of crystallites were determined at low and high cathode potentials using Scherrer relation [8] in order to explain the differences of structures in the morphological images shown in Fig. 4. The grain sizes were calculated for the highest two peak intensities of the (111) fcc and (110) bcc orientations for the films deposited at lowest ($-1.8$ V) and highest ($-2.7$ V) cathode potentials. Average grain sizes of the films at $-1.8$ V are calculated as 20 and 27 nm and at $-2.7$ V they are 26 and 25 nm, respectively.

The field was applied both parallel and perpendicular to the current flowing in the film plane to measure the longitudinal
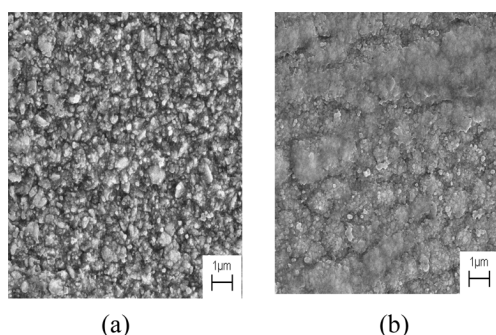
Fig. 4. Micrographs of the films deposited at (a) low ($-1.8$ versus SCE) and (b) high ($-2.7$ V versus SCE) cathode potentials.
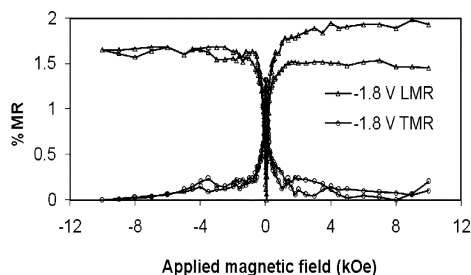


Fig. 5. MR curves of the film deposited at $-1.8$ V versus SCE.



Fig. 6. Hysteresis loops of the film produced at $-1.8$ V versus SCE.

(LMR) and transverse magnetoresistance (TMR), respectively. The percentage change of the MR(%) as a function of the magnetic field was calculated by equation $\mathrm{MR}(\%) = \{[R(H) - R_{\min}]/R_{\min}\} \times 100$, where $R(H)$ is the value of resistance at any magnetic field $H$, and $R_{\min}$ is the value at the field where the resistance is minimum. All Co–Fe films exhibited anisotropic magnetoresistance (AMR) regardless of the cathode potentials. The results of MR measurements are listed in Table I. The increase of the LMR and the decrease of the TMR were seen with the increase of magnetic field. Fig. 5 shows MR of the film at $-1.8$ V, and the LMR is 1.6% and TMR is 1.3%. The magnitude in LMR of the films increased from 2.5% to 4.1% with the change of the preferred orientation caused by the increase of the cathode potential from $-2.0$ to $-2.7$ V, whereas TMR stayed almost constant (2.1%–2.4%) (see Table I).

To obtain the magnetic properties of the films, hysteresis loops were measured at parallel and perpendicular to the film plane at room temperature. The magnetic measurements results are presented in Table I. As an example, Fig. 6 shows the hysteresis loops of the film produced at $-1.8$ V. Saturation magnetization, $M_s$ is 1341 emu/cm$^3$ and coercivity, $H_c$ is 46.98 Oe for the film grown at $-1.8$ V. $M_s$ increases to 1633 emu/cm$^3$ as the cathode potential increases to $-2.7$ V, and the coercivity decreases to 31.74 Oe (see Table I). The $M_s$ values were affected by the change of the fcc to bcc phase ratio caused by the variation of the Co content. The difference between the grain sizes was larger at the high coercivity films deposited at $-1.8$ V whereas the close grain sizes may cause the low coercivity for the films at $-2.7$ V. The in-plane loops have a higher saturation magnetization and lower coercivity than the perpendicular loops. This indicates that the easy axis direction of the magnetization is parallel to the film plane. As a result of demagnetizing effect, the shape anisotropy dictates the film must have planar easy axis. The planar magnetization
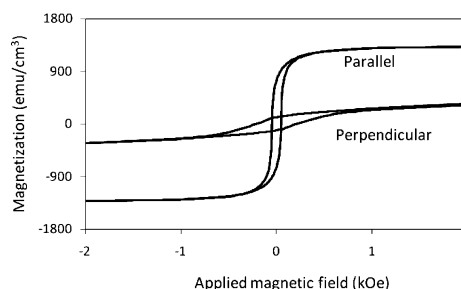
loops were observed for all films. The variations in the magnetic properties are compatible with the MR findings.

## IV. CONCLUSION

Co–Fe films were electrodeposited on polycrystalline Ti substrates at different cathode potentials ($-1.8$ to $-2.7$ V). The films were found to have the fcc + bcc mix phase but the magnitude of the phase ratio is found to be dependent on the cathode potentials. In addition, the slight increase of Co content in the films should be considered as the deposition potential increases. All films exhibited AMR. The LMR magnitude increased and the saturation magnetization and coercivity showed variations with the increase of the cathode potentials.

## REFERENCES

[1] L. T. Romankiw and D. A. Thompson, "Thin Film Inductive Transducer," U.S. Patent 4295173, Oct. 13, 1981.
[2] T. Osaka, T. Asahi, J. Kawaji, and T. Yokoshima, "Development of high-performance magnetic thin film for high-density magnetic recording," *Electrochimica Acta*, vol. 50, pp. 4576–4585, 2005.
[3] J. A. Koza, M. Uhlemann, A. Gebert, and L. Schultz, "The effect of magnetic fields on the electrodeposition of CoFe alloys," *Electrochimica Acta*, vol. 53, pp. 5344–5353, 2008.
[4] L. Ricq, F. Lallemand, M. P. Gigandet, and J. Pagetti, "Influence of sodium saccharin on the electrodeposition and characterization of CoFe magnetic film," *Surf. Coat. Technol.*, vol. 138, pp. 278–283, 2001.
[5] F. R. Bent and L. H. Mascaro, "Analysis of the initial stages of electrocrystallization of Fe, Co and Fe-Co alloys in chloride solutions," *J. Braz. Chem. Soc.*, vol. 13, no. 4, pp. 502–509, 2002.
[6] Sahari, A. Azizi, G. Schmerber, M. Abes, J. P. Bucher, and A. Dinia, "Electrochemical nucleation and growth of Co and CoFe alloys on Pt/Si substrates," *Catalysis Today*, vol. 113, no. 3–4, pp. 257–262, 2006.
[7] F. Lallemand, L. Ricq, M. Wery, P. Berçot, and J. Pagetti, "Kinetic and morphological investigation of Co–Fe alloy electrodeposition in the presence of organic additives," *Surf. Coat. Technol.*, vol. 179, no. 1–2, pp. 314–323, 2004.
[8] B. D. Cullity, *Elements of X-Ray Diffraction*. Reading, MA: Addison-Wesley, 1978.